Supporting Information

Focused Electron Beam-Induced Deposition of Oblique Co and Fe Nanowires: Compositional and Magnetic Characterisation for Functional 3D Nanostructures

Authors: Aurys Šilinga[1], Keir L. Edgar[1], András Kovács[2], Stephen McVitie[1], Rafal E. Dunin-Borkowski[2], Kayla Fallon[1], and Trevor P. Almeida[1].

[1]. SUPA, School of Physics and Astronomy, University of Glasgow, Glasgow, G12 8QQ, United Kingdom.
[2]. Ernst Ruska-Centre for Microscopy and Spectroscopy with Electrons, Forschungszentrum, Jülich, 52425 Jülich, Germany

Emails: a.silinga.1@research.gla.ac.uk (Aurys Šilinga), Trevor.Almeida@glasgow.ac.uk (Trevor Almeida)

Downloaded from pubs.acs.org/aanmf6/article-supplement/5444543/pdf/an6c02497_si_001/ by FORSCHUNGZENTRUM JUELICH user on 16 October 2026

Contents

1. Atlas of individual FEBID NW characterisations 1
Dataset “Co_30kV_↑” 2
Dataset “Co_5kV_↑” 2
Dataset “Co_anneal_30kV_↑” 3
Datasets “Fe_30kV_↑” and “Fe_5kV_↑” 4
Dataset “Co_30kV_↗” 5
Dataset “Co_5kV_↗” 6
Dataset “Fe_30kV_↗” 7
Dataset “Fe_5kV_↗” 8
2. Modelling of FEBID NW atomic composition 9
3. EELS spectra from the thickest and thinnest NWs 11
4. Correlations between NW geometry and metal content 12
5. Micromagnetic simulations of NWs with elliptical cross-sections 13
6. Magnetic induction in maps of thermally annealed nanowires 14
References 15

1. Atlas of individual FEBID NW characterisations

The following tables and figures uniquely identify each FEBID nanowire (NW) and display the underlying compositional maps related to the data in the main text. To facilitate comparison, figures (S1-S8) are annotated. In SEM images, solid blue lines indicate areas where STEM EELS maps are acquired for analysis. Dashed black lines represent STEM EELS maps obtained for calibration, which are not shown here but are available in the data repository. In the maps of atomic composition, blue shading corresponds to the central band, where the mean value is taken to represent average projected Co (or Fe) content. Since our data and previous works [1] do not detect ferromagnetism in NWs with less than 40% Co content, red shading indicates the presumed non-magnetic outer shell of NWs. In summary, angled FEBID NWs are asymmetric and exhibit non-trivial spatial distributions of material composition. Therefore, we show in detail how the data points in the main text were acquired.

Dataset "Co_30kV_↑"

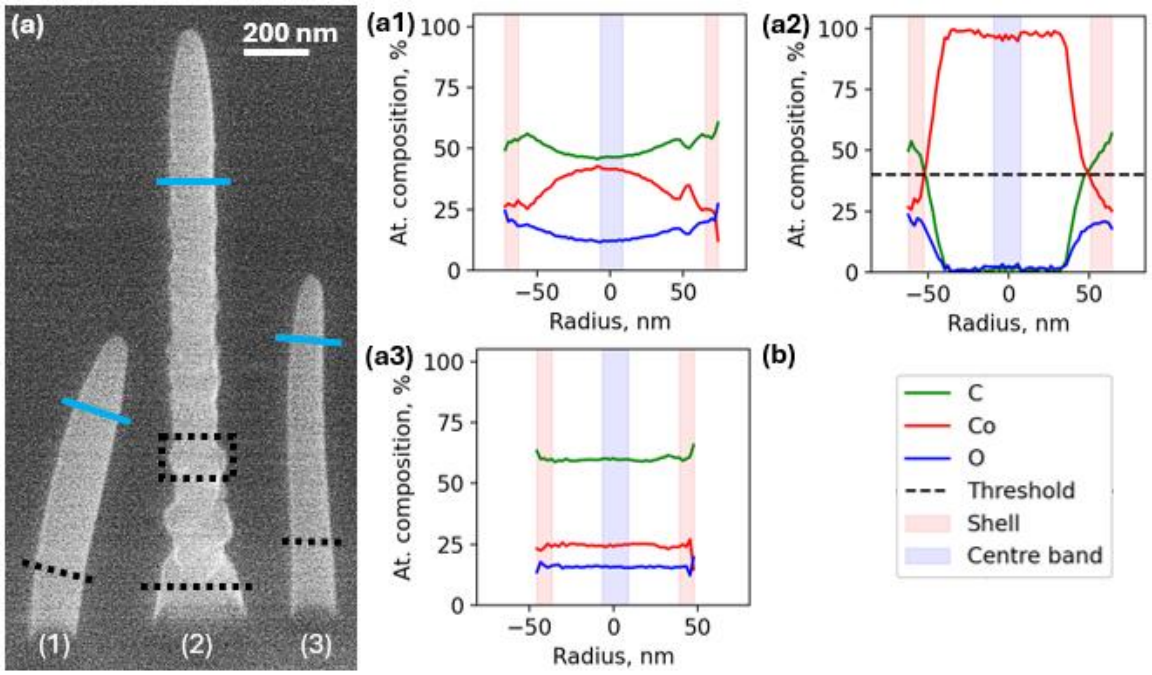


Figure S1. Characterisation of dataset "Co_30kV_↑". *(a) SEM image labelling the NWs and showing areas mapped with STEM EELS. (a1-a3) Compositional maps of the corresponding NWs. (b) Legend.*

Table S1. Deposition parameters for dataset "Co_30kV_↑". **Deposited with an out-of-focus beam.*

NW position marker in Figure S1a	(1)*	(2)	(3)*
SEM beam current, pA	690	2800	170

Dataset "Co_5kV_↑"

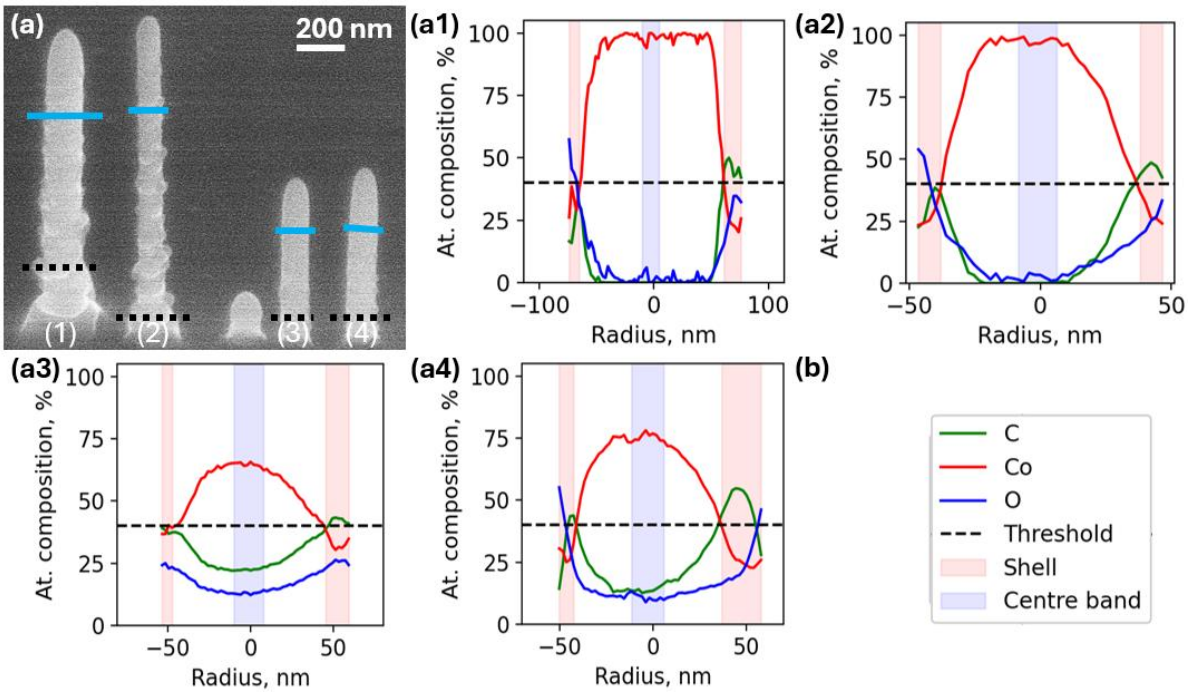


Figure S2. Characterisation of dataset "Co_5kV_↑". *(a) SEM image labelling the NWs and showing areas mapped with STEM EELS. (a1-a4) Compositional maps of the corresponding NWs. (b) Legend.*

Table S2. Deposition parameters for dataset "Co_30kV_↑".

NW position marker in Figure S2a	(1)	(2)	(3)	(4)
SEM beam current, pA	2800	690	170	340

Downloaded from pubs.acs.org/aanm6/article-supplement/5444543/pdf/an6c02497_si_001/ by FORSCHUNGZENTRUM JUELICH user on 16 October 2026

Dataset "Co_anneal_30kV_↑"

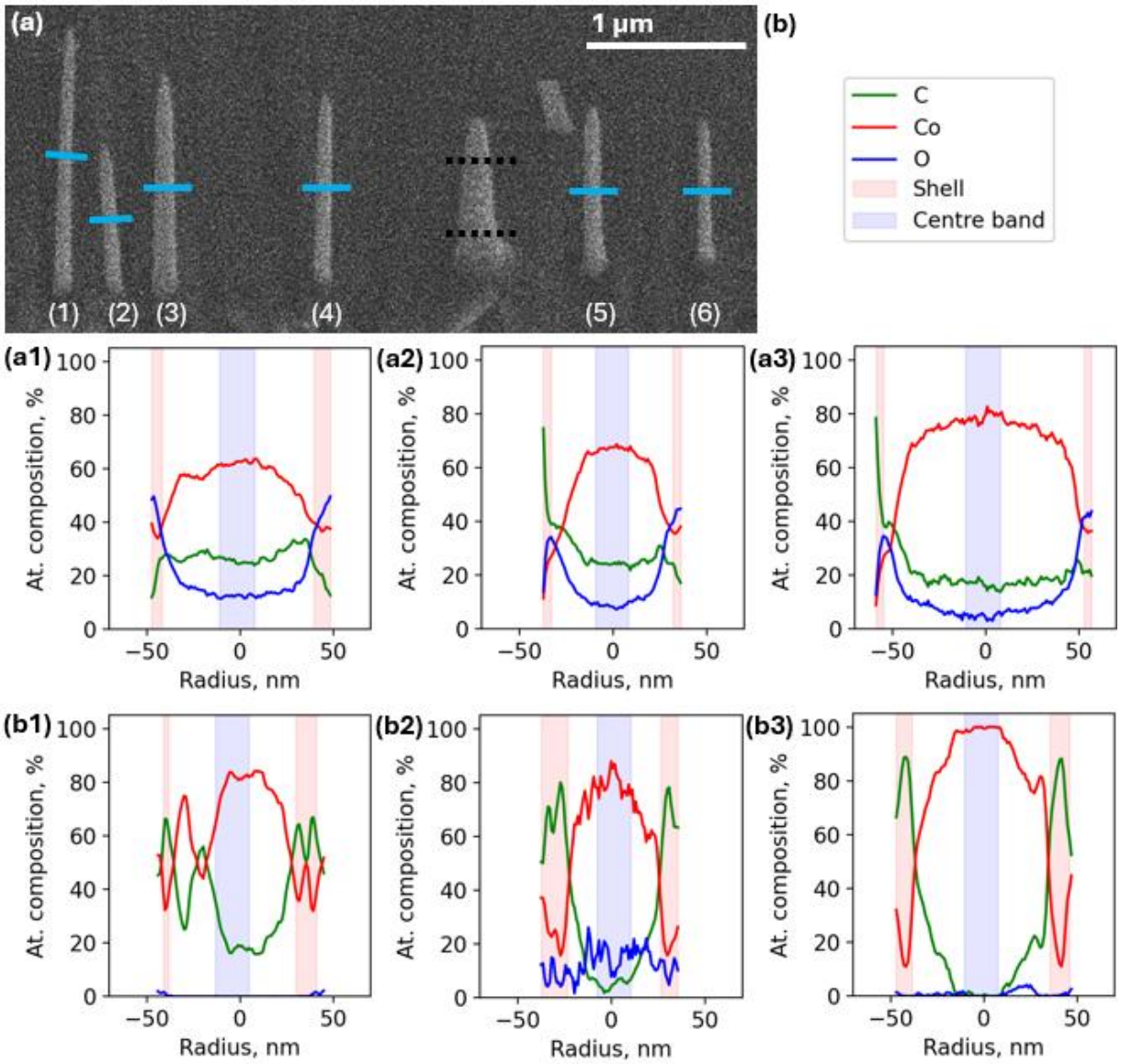


Figure S3. Structural characterisation of dataset "Co_anneal_30kV_↑". *(a) SEM image labelling the NWs and showing areas mapped with STEM EELS. (a1-a3) Compositional maps of the corresponding NWs before annealing. (b1-b3) Compositional maps of the corresponding NWs after annealing for 30 min at 350 °C. (b) Legend. This sample was characterised before and after in situ annealing inside a TEM under high vacuum.*

Table S3. Deposition parameters for dataset "Co_anneal_30kV_↑".

NW position marker in Figure S3a	(1)	(2)	(3)	(4)	(5)	(6)
SEM accelerating voltage, kV	30	30	30	15	5	5
SEM beam current, pA	86	21	340	86	86	21

Downloaded from pubs.acs.org/aanmf6/article-supplement/5444543/pdf/an6c02497_si_001/ by FORSCHUNGZENTRUM JUELICH user on 16 October 2026

Datasets "Fe_30kV_↑" and "Fe_5kV_↑"

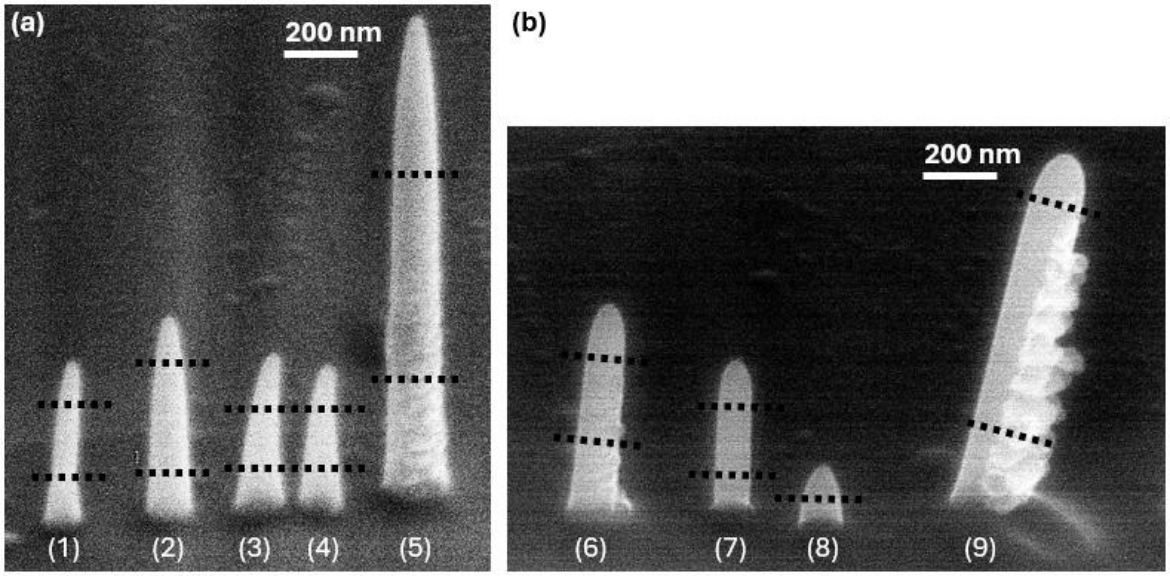


Figure S4. Characterisation of datasets "Fe_30kV_↑" and "Fe_5kV_↑". *(a-b) SEM images labelling the NWs and showing areas mapped with STEM EELS. The dataset is only required to qualitatively observe autocatalytic growth and variations of NW diameter.*

Table S4. Deposition parameters for datasets "Fe_30kV_↑" and "Fe_5kV_↑".

NW position marker in Figure S4	(1)	(2)	(3)	(4)	(5)	(6)	(7)	(8)	(9)
SEM accelerating voltage, kV	30	30	30	30	30	5	5	5	5
SEM beam current, pA	690	2800	170	170	11000	2800	690	170	11000

Downloaded from pubs.acs.org/aanmf6/article-supplement/5444543/pdf/an6c02497_si_001/ by FORSCHUNGZENTRUM JUELICH user on 16 October 2026

Dataset "Co_30kV_↗"

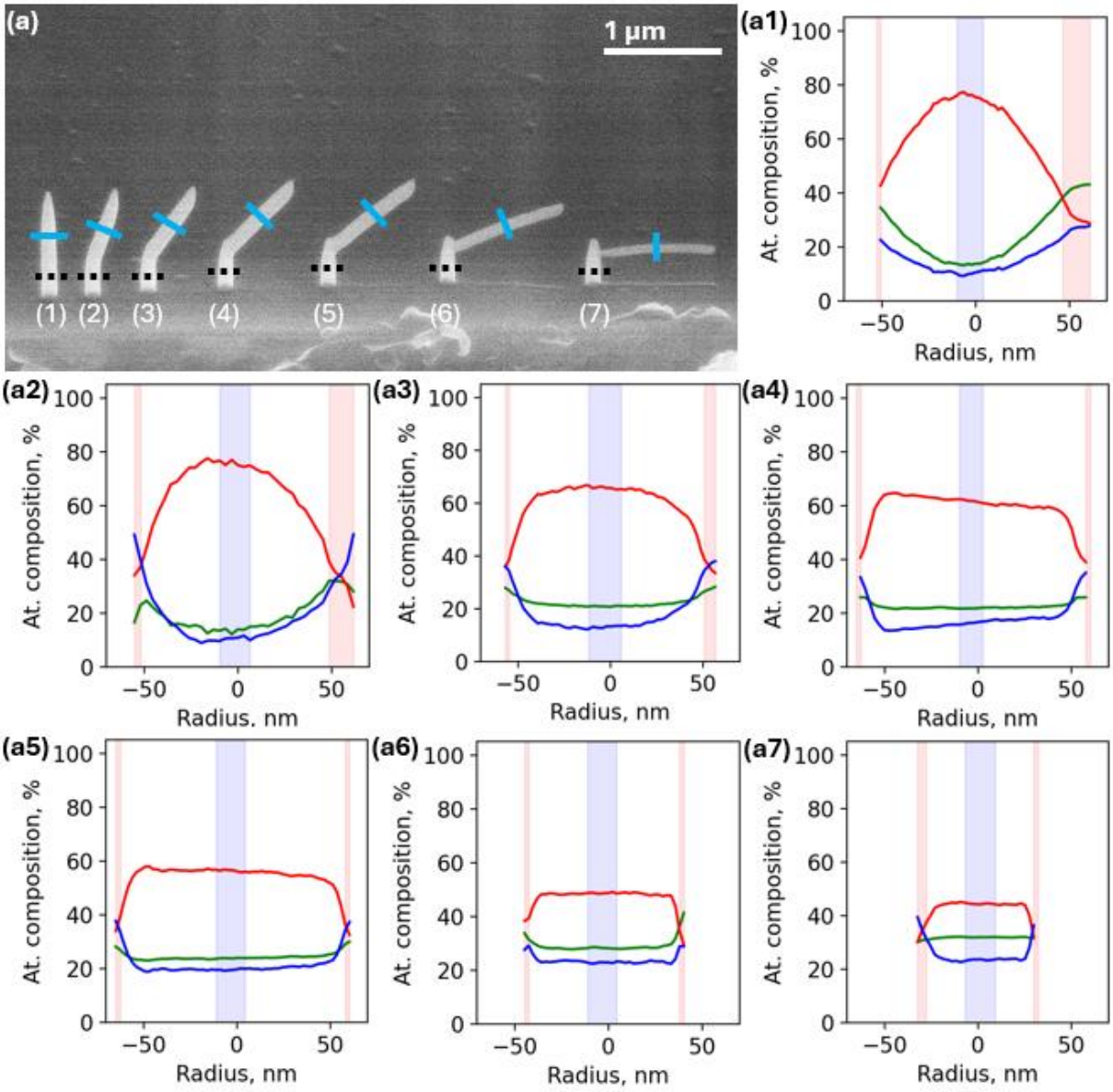


Figure S5. Structural characterisation of dataset "Co_30kV_↗". *(a) SEM image labelling the NWs and showing areas mapped with STEM EELS. (a1-a7) Compositional maps of the corresponding NWs. Uses the same legend as Figure S1.*

Downloaded from pubs.acs.org/aanmf6/article-supplement/5444543/pdf/an6c02497_si_001/ by FORSCHUNGZENTRUM JUELICH user on 16 October 2026

Dataset "Co_5kV_↗"

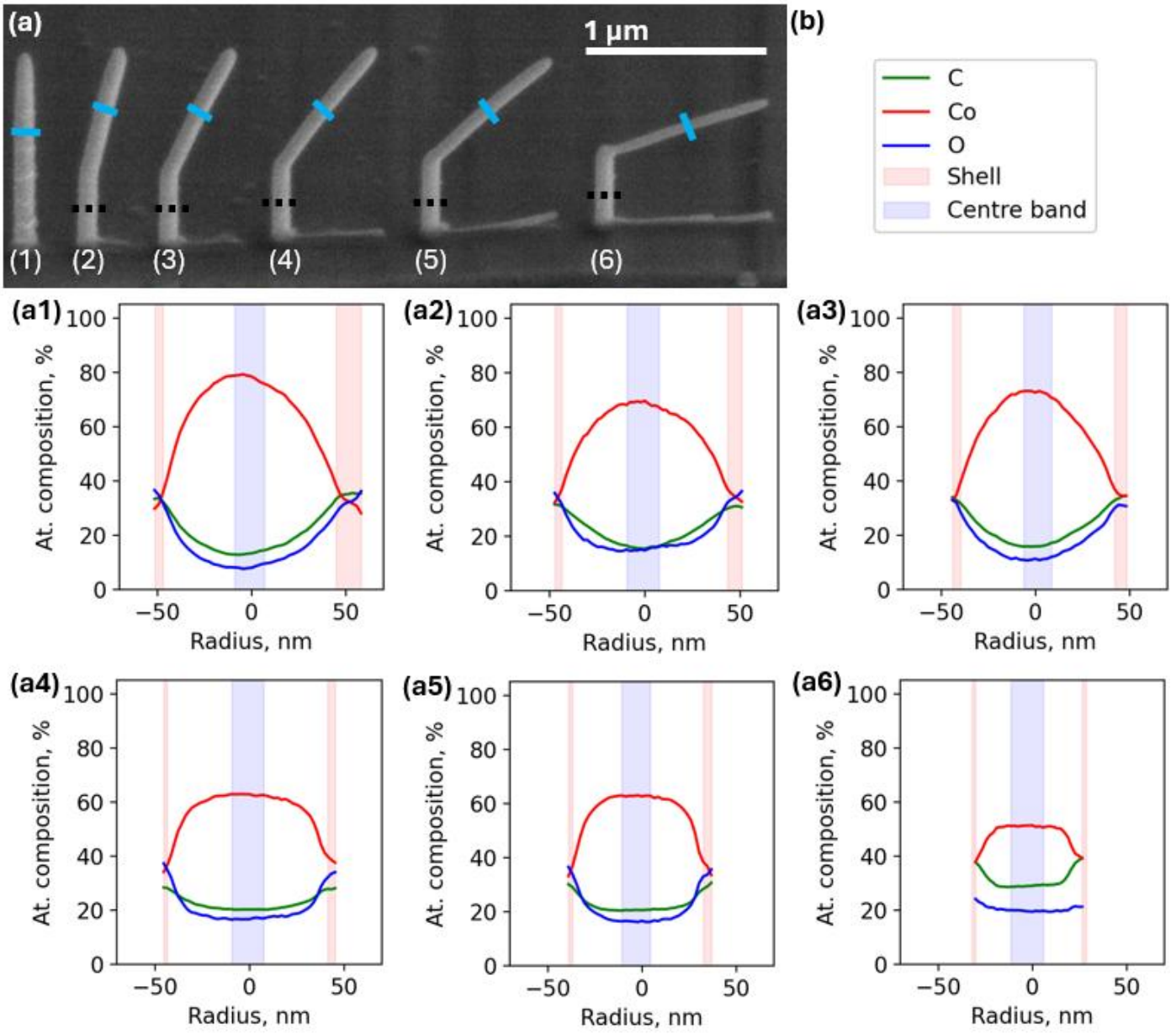


Figure S6. Structural characterisation of dataset "Co_5kV_↗". *(a) SEM image labelling the NWs and showing areas mapped with STEM EELS. (a1-a6) Compositional maps of the corresponding NWs. (b) Legend.*

Downloaded from pubs.acs.org/aanm6/article-supplement/5444543/pdf/an6c02497_si_001/ by FORSCHUNGZENTRUM JUELICH user on 16 October 2026

Dataset "Fe_30kV_↗"

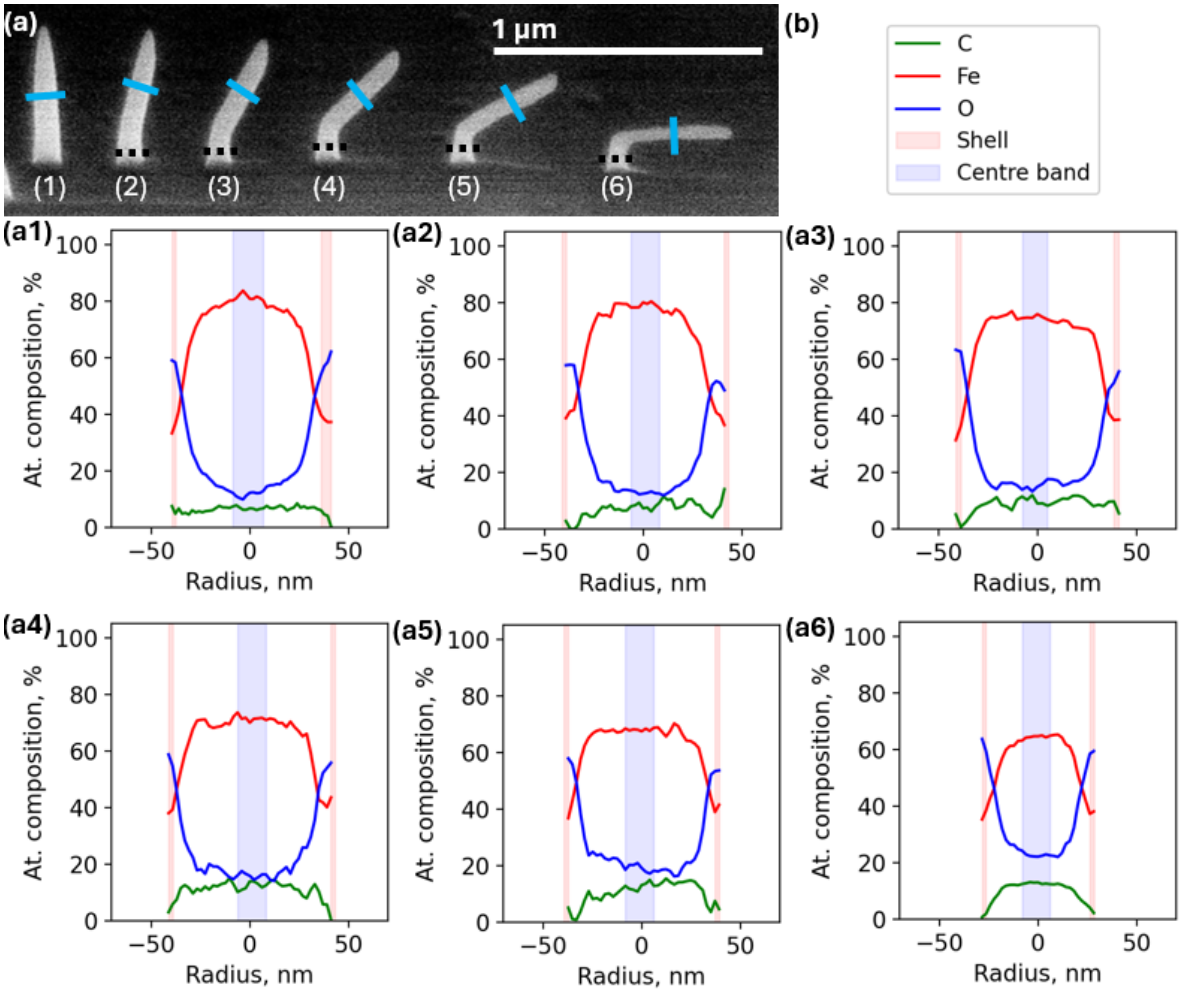


Figure S7. Structural characterisation of dataset "Fe_30kV_↗". *(a) SEM image labelling the NWs and showing areas mapped with STEM EELS. (a1-a6) Compositional maps of the corresponding NWs. (b) Legend.*

Downloaded from pubs.acs.org/aanmf6/article-supplement/5444543/pdf/an6c02497_si_001/ by FORSCHUNGZENTRUM JUELICH user on 16 October 2026

Dataset "Fe_5kV_↗"

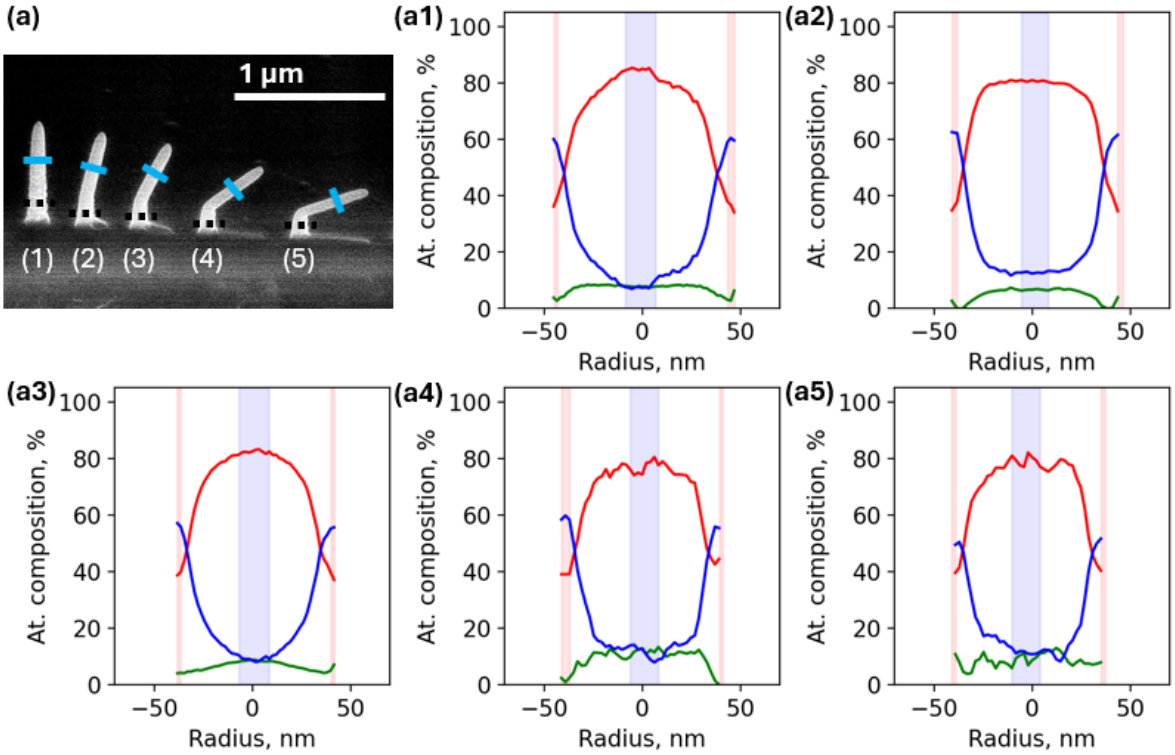


Figure S8. Structural characterisation of dataset "Fe_5kV_↗". *(a) SEM image labelling the NWs and showing areas mapped with STEM EELS. (a1-a5) Compositional maps of the corresponding NWs. Uses the same legend as Figure S1.*

Downloaded from pubs.acs.org/aanmf6/article-supplement/5444543/pdf/an6c02497_si_001/ by FORSCHUNGZENTRUM JUELICH user on 16 October 2026

2. Modelling of FEBID NW atomic composition

A quantitative model that consistently describes the internal composition of all FEBID NWs is not presented in this study, but plausible composition models for illustrative purposes are discussed. The 3D distribution of elemental composition is modelled by assuming that vertical NWs have circular cross-sections with radially varying composition. The radial distributions of Co, C, and O have been approximated by exponential functions with limited success [2], but models that correspond to experimental data more closely can be generated by modelling NWs as multi-layered cylinders. Since EELS maps are projections of the underlying 3D atomic distribution, they can be simulated based on a model of the NW and compared with experimental data, as shown in Figure S9. The model described in Figures S9a-c assumes a 25 nm radius core with 100% Co content, linearly interpolated intermediate layers, and a 10 nm shell with an average composition corresponding to the red shaded area in the figures. This model qualitatively resembles the experimental data shown in Figures S9d-f and the main text, but it does not account for asymmetry. It should be noted that the correctness of this model is not certain. Therefore, the model in the main text is shown only to illustrate the assumptions made about the 3D distribution of atomic composition inside the NWs.

The compositional model may be used to visualise how the non-magnetic NW shell affects EELS maps taken in projection. The shell composition (Figure S9g) can be estimated by arbitrarily assuming that material with <40% Co content in Figure S9b is not ferromagnetic and represents both the thickness and average composition of a hollow cylinder corresponding to the NW shell. The 40% threshold was chosen such that the cylinder wall thickness would be approximately 10 nm. The projected atomic density of the shell can be subtracted from the data (Figure S9a) to give estimates of atomic composition without the shell's contribution, as shown in Figure S9c. The same algorithm can be applied to experimental data shown in Figures S9(a-c), and in both cases indicates that if the shells were absent, Co content measurements would be approximately 10% higher. This calculation shows that the atomic metal content in the centres of the NW cores is likely higher than the maximum values shown in EELS maps acquired in projection.

Downloaded from pubs.acs.org/aanmf6/article-supplement/5444543/pdf/an6c02497_si_001/ by FORSCHUNGZENTRUM JUELICH user on 16 October 2026

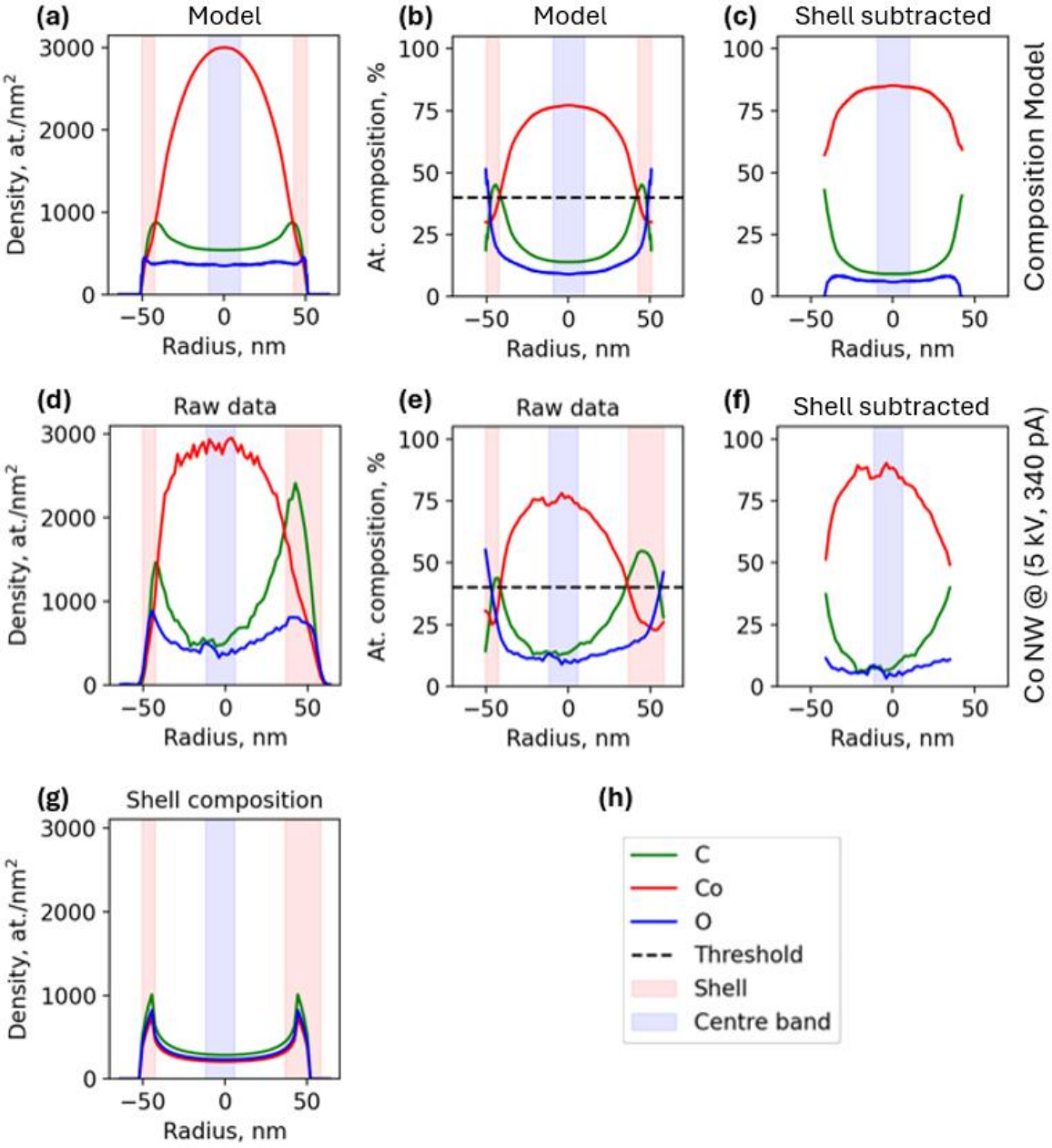


Figure S9. Comparison between simulation and measurement of atomic composition in dataset "Co_5kv_↑" wire (8). *(a)-(c) A radially symmetric simulation, attempting to reproduce experimental data in (d)-(f). (d), (e) Experimental data. (g) An estimate of the composition of the outer shell of the NW. (f) Experimental data after subtracting the contribution of the assumed shell. (h) Legend.*

Downloaded from pubs.acs.org/aanmf6/article-supplement/5444543/pdf/an6c02497_si_001/ by FORSCHUNGZENTRUM JUELICH user on 16 October 2026

3. EELS spectra from the thickest and thinnest NWs

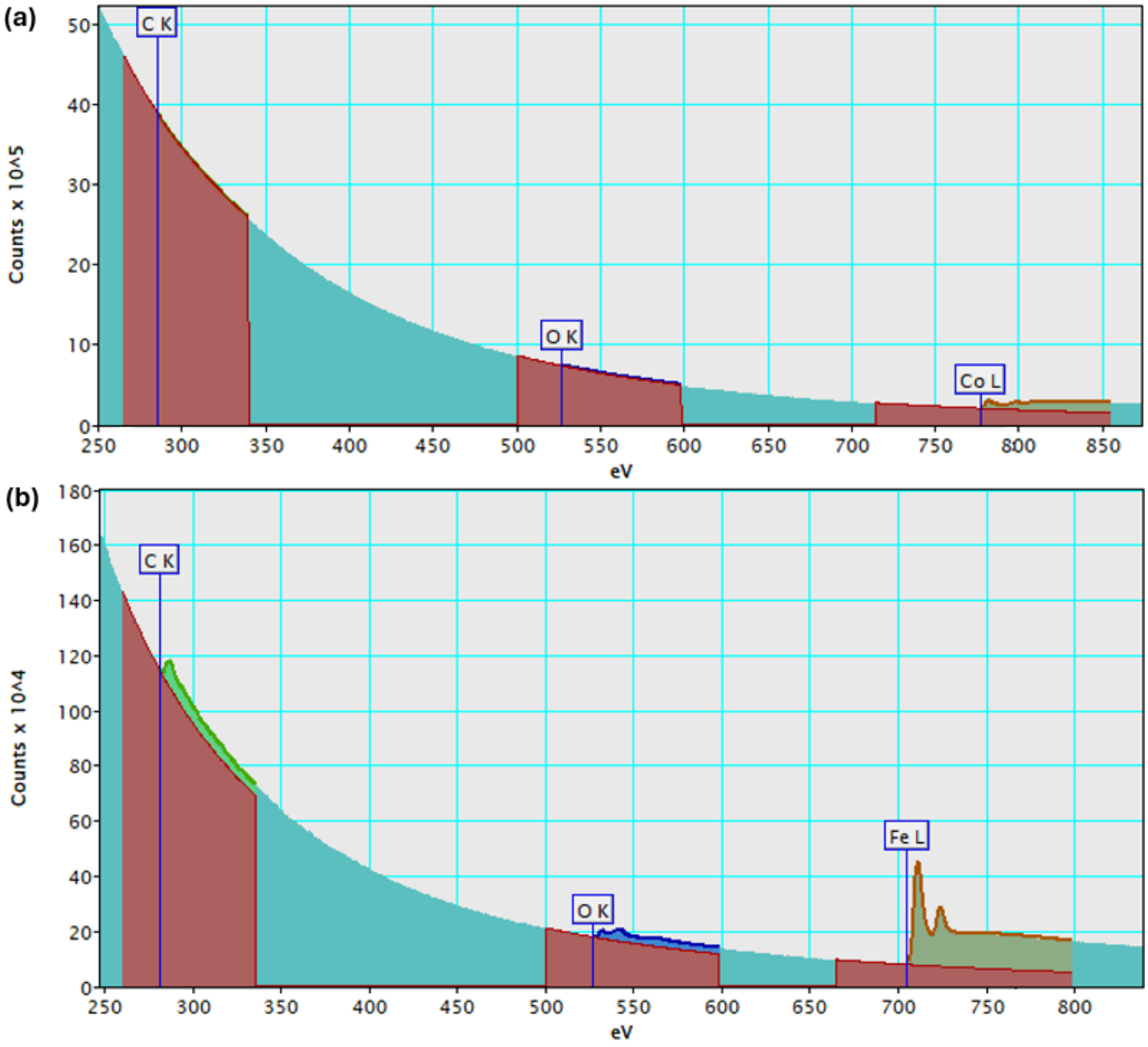


Figure S10. EELS spectra from the 20 nm central bands of NWs of different thickness. *(a) NW at position (1) in dataset "Co_5kV_↑", with 130 nm projected thickness. (b) NW at position (6) in dataset "Fe_30kV_↗", with 30 nm projected thickness. (a) and (b) correspond to NWs with the greatest and the lowest projected thickness in all datasets, respectively.*

Downloaded from pubs.acs.org/aanmf6/article-supplement/5444543/pdf/an6c02497_si_001/ by FORSCHUNGZENTRUM JUELICH user on 16 October 2026

4. Correlations between NW geometry and metal content

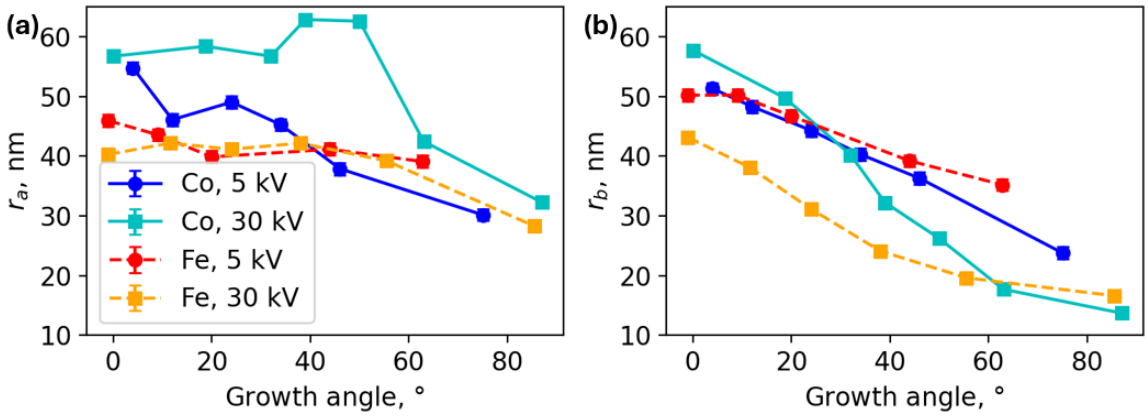


Figure S11. Comparison of cross-section semi-axes in oblique NWs. *(a) Major semi-axis (r_a). (b) Minor semi-axis (r_b). For all datasets, the minor axis depends more strongly on growth angle.*

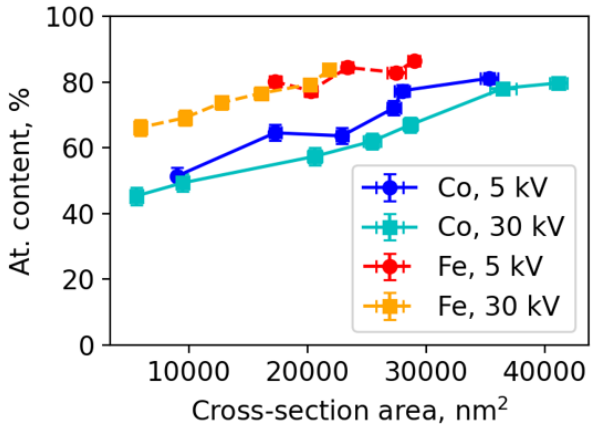


Figure S12. Correlation between atomic content of metal atoms and NW cross-sectional area. *NW geometry can affect the atomic content measurements in all datasets.*

Downloaded from pubs.acs.org/aanmf6/article-supplement/5444543/pdf/an6c02497_si_001/ by FORSCHUNGZENTRUM JUELICH user on 16 October 2026

5. Micromagnetic simulations of NWs with elliptical cross-sections

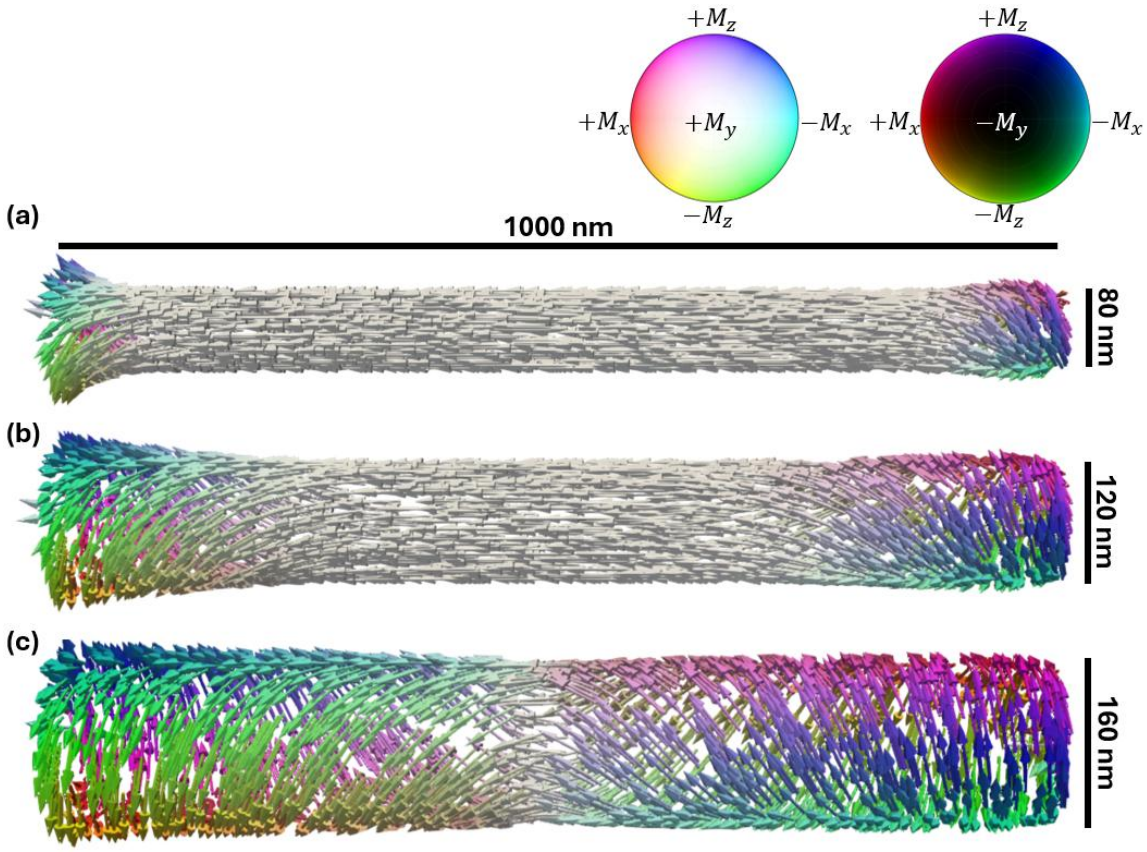


Figure S13. Micromagnetic simulations of FEBID Co cylinders. *(a), (b), (c) correspond, respectively, to 80 nm,120 nm, and 160 nm diameter cylinders. In the energetically stable configuration, cylinders with diameters below 150 nm are predominantly magnetised parallel to the long axis. The inset arrows correspond to principal directions in the colour map. Simulation parameters are described in the main text.*

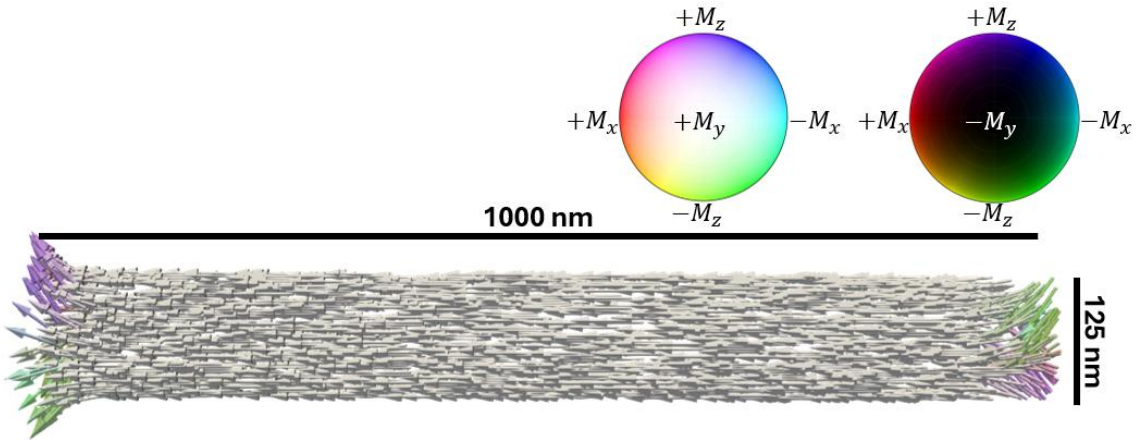


Figure S14. Micromagnetic simulation of a FEBID Co cylinder with an elliptical cross-section. *The NW length is 1000 nm, and cross-section radii are r_a = 62.5 nm and r_b=25 nm. This corresponds to the most elongated NW cross-section geometry in the experimental dataset and shows that the magnetisation is predominantly aligned along the NW long axis. Simulation parameters are described in the main text.*

Downloaded from pubs.acs.org/aanmf6/article-supplement/5444543/pdf/an6c02497_si_001/ by FORSCHUNGZENTRUM JUELICH user on 16 October 2026

6. Magnetic induction in maps of thermally annealed nanowires

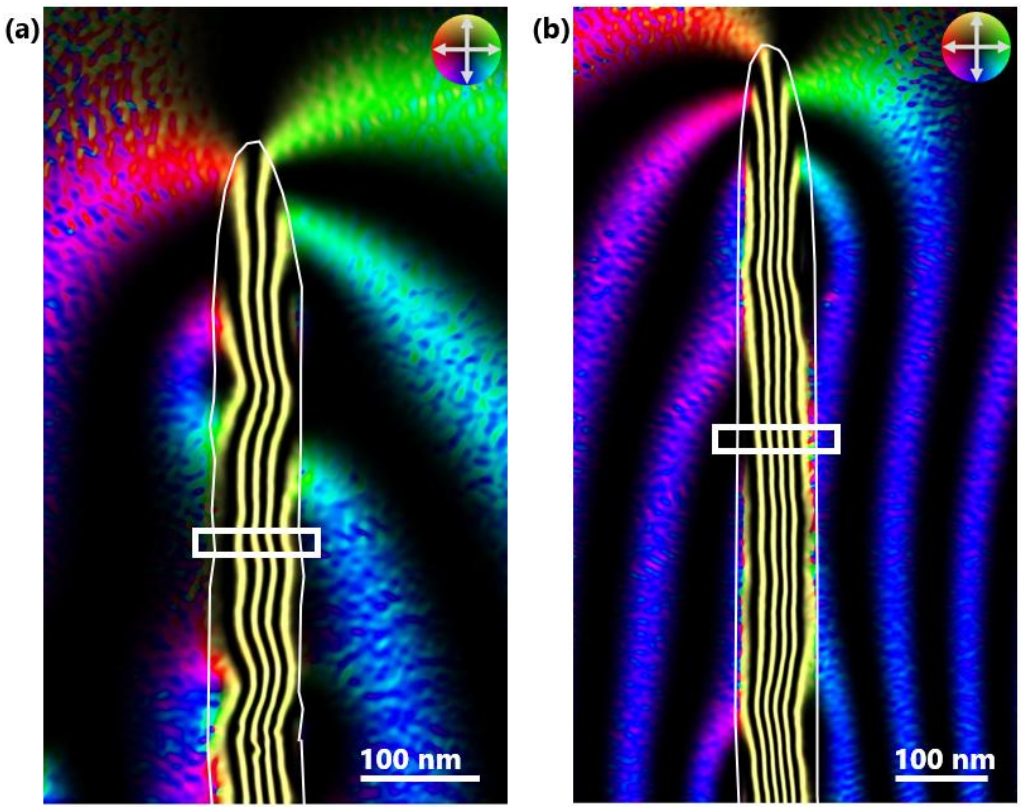


Figure S15. Magnetic induction maps of Co NWs annealed at 350 °C for 30 min. *(a) and (b) were deposited using 21 pA and 86 pA beam currents, respectively. Contour spacing is 1.3 rad, and line traces of magnetic phase shift are from areas corresponding to the white boxes. These NWs correspond to positions (6) and (4) in dataset "Co_anneal_30kV_↑, respectively.*

Downloaded from pubs.acs.org/aanmf6/article-supplement/5444543/pdf/an6c02497_si_001/ by FORSCHUNGZENTRUM JUELICH user on 16 October 2026

References

[1] Magén, C.; Pablo-Navarro, J.; De Teresa, J. M. Focused-Electron-Beam Engineering of 3D Magnetic Nanowires. Nanomaterials 2021, 11 (2), 402. https://doi.org/10.3390/nano11020402.

[2] Keller, L.; Al Mamoori, M. K. I.; Pieper, J.; Gspan, C.; Stockem, I.; Schröder, C.; Barth, S.; Winkler, R.; Plank, H.; Pohlit, M.; Müller, J.; Huth, M. Direct-Write of Free-Form Building Blocks for Artificial Magnetic 3D Lattices. Sci Rep 2018, 8 (1), 6160. https://doi.org/10.1038/s41598-018-24431-x.

Downloaded from pubs.acs.org/aanmf6/article-supplement/5444543/pdf/an6c02497_si_001/ by FORSCHUNGZENTRUM JUELICH user on 16 October 2026